



全球变化与地球系统科学系列

Series in Global Change and Earth System Science

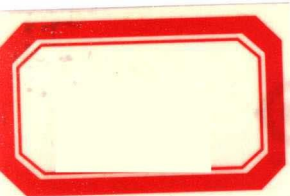
Seismic Imaging, Fault Damage and Heal

地震成像与断裂破碎和愈合

Yong-Gang Li (Ed.)



高等教育出版社
HIGHER EDUCATION PRESS



全球变化与地球系统科学系列

Series in Global Change and Earth System Science

Seismic Imaging, Fault Damage and Heal

地震成像与断裂破碎和愈合

Yong-Gang Li (Ed.)



DIZHEN CHENGXIANG YU DUANLIE POSUI HE YUHE



高等教育出版社·北京
HIGHER EDUCATION PRESS BEIJING

图书在版编目（CIP）数据

地震成像与断裂破碎和愈合 = Seismic Imaging, Fault Damage and Heal: 英文 / (美) 酈永刚主编. —北京: 高等教育出版社, 2014. 3
ISBN 978-7-04-039098-8

I. ①地… II. ①酈… III. ①地震层析成像 - 研究 - 英文 IV. ①P631.4

中国版本图书馆 CIP 数据核字 (2013) 第 308025 号

策划编辑	关 焱	责任编辑	关 焱	封面设计	张 楠	版式设计	王艳红
责任校对	刁丽丽	责任印制	韩 刚				

出版发行	高等教育出版社	咨询电话	400-810-0598
社 址	北京市西城区德外大街4号	网 址	http://www.hep.edu.cn
邮政编码	100120		http://www.hep.com.cn
印 刷	北京汇林印务有限公司	网上订购	http://www.landrace.com
开 本	787mm × 1092mm 1/16		http://www.landrace.com.cn
印 张	24.25	版 次	2014 年 3 月第 1 版
字 数	520 千字	印 次	2014 年 3 月第 1 次印刷
购书热线	010-58581118	定 价	139.00 元

本书如有缺页、倒页、脱页等质量问题, 请到所购图书销售部门联系调换
版权所有 侵权必究
物 料 号 39098-00

Preface

This book is the second monograph of the earth science specializing in computational, observational and interpretational seismology and geophysics, containing the full-3D waveform tomography method and its application; beamlets and curvelets method for wavefield representation, propagation and imaging; two-way coupling of solid-fluid with discrete element model and lattice Boltzmann model; fault-zone trapped wave observations and 3-D finite-difference synthetics for high-resolution imaging subsurface rupture zone segmentation and bifurcation; fault rock damage and heal associated with earthquakes in California and New Zealand; characterization of pre-shock accelerating moment release with careful considerations in processing and analysis of seismicity using earthquake catalogues; and statistical modeling of earthquake occurrences based on the ultra-low frequency ground electric signals. Each chapter in this book includes the detailed discussion of the state-of-the-art method and technique with their applications in case study. The editor approaches this as a broad interdisciplinary effort, with well-balanced observational, metrological and numerical modeling aspects. Linked with these topics, the book highlights the importance for imaging the crustal complex structures and internal fault-zone rock damage at seismic depths that are closely related to earthquake occurrence and physics.

Researchers and graduate students in geosciences will broaden their horizons about advanced methodology and technique applied in seismology, geophysics and earthquake science. This book can be taken as an expand of the first book in the series, and covers multi-disciplinary topics to allow readers to grasp the new methods and skills used in data processing and analysis as well as numerical modeling for structural, physical and mechanical interpretation of earthquake phenomena, and to strengthen their understanding of earthquake occurrence and hazards, thus helping readers to evaluate potential earthquake risk in seismogenic regions globally. Readers of this book can make full use of the present knowledge and techniques to serve the reduction of earthquake disasters.

Contents

Seismic Imaging, Fault Damage and Heal: An Overview —	1
References —	10

1 Applications of Full-Wave Seismic Data Assimilation (FWSDA) — 15

1.1	Numerical Solutions of Seismic Wave Equations —	16
1.1.1	Stable Finite-Difference Solutions on Non-Uniform, Discontinuous Meshes —	18
1.1.2	Accelerating Finite-Difference Methods Using GPUs —	22
1.1.3	The ADER-DG Method —	26
1.1.4	Accelerating the ADER-DG Method Using GPUs —	29
1.2	Automating the Waveform Selection Process for FWSDA —	41
1.2.1	Seismogram Segmentation —	42
1.2.2	Waveform Selection —	49
1.2.3	Misfit Measurement Selection —	50
1.2.4	Fréchet Kernels for Waveforms Selected in the Wavelet Domain —	51
1.3	Application of FWSDA in Southern California —	55
1.3.1	Waveform Selection on Ambient-Noise Green's Functions —	57
1.3.2	Waveform Selection on Earthquake Recordings —	59
1.3.3	Inversion Results after 18 times Adjoint Iteration —	60
1.4	Summary and Discussion —	63
	References —	65

2 Wavefield Representation, Propagation and Imaging Using Localized Waves: Beamlet, Curvelet and Dreamlet — 73

2.1	Introduction —	74
2.2	Phase-Space Localization and Wavelet Transform —	77
2.2.1	Time-Frequency Localization —	78
2.2.2	Time-Scale Localization —	81
2.2.3	Extension and Generalization of Time-Frequency, Time-Scale Localizations —	82
2.3	Localized Wave Propagators: From Beam to Beamlet —	85
2.3.1	Frame Beamlets and Orthonormal Beamlets —	87
2.3.2	Beamlet Spreading, Scattering and Wave Propagation in the Beamlet Domain —	90

2.3.3	Beam Propagation in Smooth Media with High-Frequency Asymptotic Solutions — 96
2.3.4	Beamlet Propagation in Heterogeneous Media by the Local Perturbation Approach — 101
2.4	Curvelet and Wave Propagation — 106
2.4.1	Curvelet and Its Generalization — 106
2.4.2	Fast Digital Transforms for Curvelets and Wave Atoms — 110
2.4.3	Wave Propagation in Curvelet Domain and the Application to Seismic Imaging — 110
2.5	Wave Packet: Dreamlets and Gaussian Packets — 112
2.5.1	Physical Wavelet and Wave-Packets — 112
2.5.2	Dreamlet as a Type of Physical Wavelet — 116
2.5.3	Seismic Data Decomposition and Imaging/Migration Using Dreamlets — 119
2.5.4	Gaussian Packet Migration and Paraxial Approximation of Dreamlet — 123
2.6	Conclusions — 130
	Acknowledgement — 131
	References — 132

3 Two-way Coupling of Solid-fluid with Discrete Element Model and Lattice Boltzmann Model — 143

3.1	Introduction — 143
3.2	Discrete Element Method and the ESyS-Particle Code — 146
3.2.1	A Brief Introduction to the Open Source DEM Code: The ESyS-Particle — 147
3.2.2	The Basic Equations — 147
3.2.3	Contact Laws and Particle Interaction — 148
3.2.4	Fracture Criterion — 150
3.3	Lattice Boltzmann Method — 151
3.3.1	The Basic Principle of LBM — 151
3.3.2	Boundary Conditions of LBM — 152
3.3.3	A Brief Introduction to the Open Source LBM Code: OpenLB — 156
3.4	Two-way Coupling of DEM and LBM — 156
3.4.1	Moving Boundary Conditions — 157
3.4.2	Curved Boundary Conditions — 157
3.4.3	Implementation of Darcy Flow in LBM — 160
3.5	Preliminary Results — 161
3.5.1	Bonded Particles Flow in Fluid — 161
3.5.2	Fluid Flow in the Fractures — 162
3.5.3	Hydraulic Fracture Simulation — 164
3.6	Discussion and Conclusions — 166
	Acknowledgement — 167
	References — 167

4	Co-seismic Damage and Post-Mainshock Healing of Fault Rocks at Landers, Hector Mine and Parkfield, California Viewed by Fault-Zone Trapped Waves —173
4.1	Introduction — 173
4.2	Rock Damage and Healing on the Rupture Zone of the 1992 <i>M</i> 7.4 Landers Earthquake — 176
4.2.1	Landers Rupture Zone Viewed with Fault-Zone Trapped Waves — 176
4.2.2	Fault Healing at Landers Rupture Zone — 183
4.2.3	Additional Damage on the Landers Rupture Zone by the Nearby Hector Mine Earthquake — 192
4.3	Rock Damage and Healing on the Rupture Zone of the 1999 <i>M</i> 7.1 Hector Mine Earthquake — 194
4.3.1	Hector Mine Rupture Zone Viewed with FZTWs — 194
4.3.2	Fault Healing at Hector Mine Rupture Zone — 204
4.4	Rock Damage and Healing on the San Andreas Fault Associated with the 2004 <i>M</i> 6 Parkfield Earthquake — 208
4.4.1	Low-Velocity Damaged Structure of the San Andreas Fault at Parkfield from Fault Zone Trapped Waves — 209
4.4.2	Seismic Velocity Variations on the San Andreas Fault Caused by the 2004 <i>M</i> 6 Parkfield Earthquake — 218
4.4.3	Discussion — 237
4.5	Conclusion — 239
	Acknowledgment — 242
	References — 242
5	Subsurface Rupture Structure of the <i>M</i>7.1 Darfield and <i>M</i>6.3 Christchurch Earthquake Sequence Viewed with Fault-Zone Trapped Waves —249
5.1	Introduction — 250
5.2	The Data and Waveform Analyses — 256
5.2.1	The FZTWs Recorded for Aftershocks along Darfield/Greendale Rupture Zone — 264
5.2.2	The FZTWs Recorded for Aftershocks along Christchurch/Port Hills Rupture Zone — 277
5.3	Subsurface Damage Structure Viewed with FZTWs — 288
5.4	3-D Finite-Difference Simulations of Observed FZTWs — 294
5.5	Conclusion and Discussion — 306
	Acknowledgment — 314
	References — 314
6	Characterizing Pre-shock (Accelerating) Moment Release: A Few Notes on the Analysis of Seismicity —323
6.1	Introduction — 323
6.2	The ‘Interfering Events’ and the ‘Eclipse Method’ — 325
6.3	Comparing with Linear Increase: The BIC Criterion — 327

6.4	The Time-Space- M_C Mapping of the Scaling Coefficient, $m(T, R, M_C)$ — 328
6.5	Removal of Aftershocks and the ‘De-clustered Benioff Strain’ — 331
6.6	‘Crack-like’ Spatial Window for Great Earthquakes: The 2008 Wenchuan Earthquake — 335
6.7	Looking into a Finite Earthquake Rupture: The 2004 Sumatra-Andaman Earthquake — 338
6.8	Using Seismic Moment Tensors to Investigate the Moment Release: $AM_{ij}R$ before the 2011 Tohoku Earthquake? — 340
6.9	Concluding Remarks and Discussion — 344
6.10	Appendix: The Magnitude Conversion Problem, and the Completeness of an Earthquake Catalogue — 345
6.10.1	Magnitudes — 345
6.10.2	Conversion of Magnitudes — 346
6.10.3	Completeness of an Earthquake Catalogue — 347
	References — 347
7	Statistical Modeling of Earthquake Occurrences Based on External Geophysical Observations: With an Illustrative Application to the Ultra-low Frequency Ground Electric Signals Observed in the Beijing Region — 351
7.1	Introduction — 352
7.2	The Data — 354
7.3	Model Description — 357
7.4	Results for Circles around the Individual Stations — 359
7.5	Results for the 300 km Circle around Beijing — 364
7.6	Results from the Tangshan Region — 369
7.7	Probability Gains from Forecasts Based on Electrical Signals — 371
7.8	Effect of Changes in the Background Seismicity — 373
7.9	Conclusions — 374
	References — 375

Seismic Imaging, Fault Damage and Heal: An Overview

Yong-Gang Li

This book presents state-of-the-art methods and technique in observational, computational and analytical seismology for earthquake science. Authors from global institutions present multi-disciplinary topics with case studies to illuminate high-resolution imaging of complex crustal structures and earthquake-borne fault zones by the full-3D waveform tomography, beamlets and curves of localized waves, discrete element model for fully-coupled solid-fluid, and 3-D finite-difference simulation of fault zone trapped (guided) waves observed at recent rupture zones in California and New Zealand. In addition, authors discuss the significance in characterization of the pre-shock moment release using cataloged seismicity, and statistical modeling of earthquake occurrence based on the ultra-low frequency ground electric signals. All topics in this book help further understanding earthquake physics and hazard assessment in global seismogenic regions.

The detailed crustal structure and physical properties of fault network are of great interest because of the factors that control the occurrence and dynamic rupture in earthquake. Observations suggest that the crustal complexity may segment fault zones (Aki, 1984; Malin *et al.*, 1989; Ellsworth, 1990; Beck and Christensen, 1991) or control the timing of moment release in earthquakes (Harris and Day, 1993; Wald and Heaton, 1994). Rupture models have been proposed that involved variations in fluid pressure over the earthquake cycle (Hickman *et al.*, 1995; Blanpied *et al.*, 1992). Geometrical, structural, and rheological fault discontinuities, caused by the spatial variations in strength and stress, will affect the earthquake rupture (e.g., Wesson and Ellsworth, 1973; Das and Aki, 1977; Rice, 1980; Day, 1984; Duan, 2012). Rupture segmentation is often related to fault bends, step-overs, branches, and terminations that have been recognized by surface mapping (e.g., Sieh *et al.*, 1993; Johnson *et al.*, 1994), exhumation (e.g., Chester *et al.*, 1993), and seismic profiling and tomography

(e.g., Lees and Malin, 1990; Thurber *et al.*, 2004). In order to relate present-day crustal stresses and fault motions to the geological structures formed by previous ruptures, we must understand the evolution of fault systems on many spatial and temporal scales in the complex earth crust.

Because the fault plane is thought to be a weakness plane in the earth crust, it facilitates slip to occur under the prevailing stress orientation. As suggested by laboratory experiments, shear faulting is highly resisted in brittle material and proceeds as re-activated faults along surfaces which have already encountered considerable damage (e.g., Dieterich, 1997; Marone, 1998). Field evidence shows that the rupture plane of slip on a mature fault occurs at a more restricted position, the edge of damage zone at the plane of contact with the intact wall rock (Chester *et al.*, 1993; Chester and Chester, 1998). Assuming that this is an actual picture of rupture preparation on the major faults, high-resolution defining the crustal complex and internal damage structure of faults as well as their temporal variations in physical property are challenging work in earthquake science.

Monitoring seismic events and other physical field related to the principal rupture plane would be crucial for earthquake prediction. The slip of these events in series with the main fault is most likely to load the principal slip plane to a point of a major through-going rupture. In these circumstances, it is important to image where the principal fault plane is accompanied with damage zone at depth. Detailing the crustal structure and local variations in seismic velocities has implications for near-fault hazards and expected ground shaking. Greater amplitude shaking is expected near faults due to both proximity to the fault and localized amplification in damaged material. Examining the geometry and physical properties of fault zones as well as the crustal complex structure will help us understand the origin of spatial and temporal variations in rock damage and the evolution of heterogeneities in stress and strain in a seismogenic region.

Other geophysical parameters, such as signals from the ultra-low frequency ground electric field, can be applied for modeling earthquake occurrence. For instance, the version of Ogata's Lin-Lin algorithm (Ogata, 1988) presented in this book is useful for examining the influence of an explanatory signal on the occurrence of earthquakes in a stochastic point process. The statistical models based on observations of these signals allow to forecast earthquakes in its associated circle.

In this book, we introduce the new methodology and technology used in data assimilation for defining subsurface complexity, seismically imaging the multi-scale crustal heterogeneity and fault zone geometry, characterizing fault damage magnitude and heal progression, and its physical properties with high-resolution. We also introduce a sophisticated discrete element model with solid-fluid coupling mechanics for earthquake fracture zone rheological simulation, and the pre-

shock accelerating moment release (AMR) model related to the critical-point-like behavior of earthquake preparation. This book includes seven chapters.

Chapter 1: “Applications of Full-Wave Seismic Data Assimilation (FWSDA)” by Dawei Mu, En-Jui Lee and Po Chen.

In the first volume of this book series, Po Chen (2012) introduced theoretical background and recent advances of full-waveform seismic data assimilation (FWSDA) as well as its mathematical formulations in the framework of the various data assimilation theories. In this chapter, Mu *et al.* further discuss the full-wave seismological inverse, as a weakly constrained generalized inverse problem, in which the seismic wave equation with its initial and boundary conditions, the structural and source parameters and the waveform misfit measurements are all allowed to contain errors. The issues related to the applications of FWSDA in realistic seismological inverse problems are also discussed in detail.

Authors present the recent development of FWSDA that can potentially improve the efficiency of some numerical algorithms used for solving acoustic and visco-elastic seismic wave equations. To fully take advantage of the newly emerging computing hardware, algorithmic changes are needed. For the earth structure models in 3-D with highly irregular surface topography and fault structures, the efficiency and the accuracy of the wave equation solver are highly important in solving the problem in a realistic amount of time. In some of the recent successful full-3D waveform tomography applications, the waveform misfit measurements were made on selected wave packets on the seismograms. In order to achieve successful full-3D waveform tomography applications with a large amount of seismic data, the waveform selection process needs to be automated to a certain extent. Authors provide some of the latest developments in numerical solutions of the forward problem and their implementation and optimization on modern CPU-GPU hybrid parallel computing platforms. A realistic full-3D, full-wave tomography for the crustal structure in Southern California is used to illustrate the various components of FWSDA.

Chapter 2: “Wavefield Representation, Propagation and Imaging Using Localized Waves: Beamlet, Curvelet and Dreamlet” by Ru-Shan Wu and Jinghui Gao.

In this chapter, authors review phase-space localization, mainly along the line of time-frequency localization, and then phase-space localization using generalized wavelet transform applied to wave field and one-way propagator decompositions. Physically the phase-space localized propagators are beamlet or wavepacket propagators which are propagator matrices for short-range iterative propagation. When asymptotic solutions are applied to the beamlet for long-range propagation, beamlets evolve into global beams. Various asymptotic beam propagation methods have been developed in the past, such as the Gaussian beam, complex ray, coherent state, and more recently the curvelet methods. Local perturbation method for propagation in strongly heterogeneous media is

also briefly described in this chapter. Finally, authors review the development of curvlet transform and its application to propagation and imaging in comparison with the beamlet approach.

For wavefield decomposition, both beamlet and curvlet transforms have elementary functions of directional wavelets. Beamlet is a type of physical wavelet, representing an elementary wave in various wavefield decomposition schemes using localized building elements, such as coherent state, Gabor atom, Gabor-Daubechies frame vector, local trigonometric basis function. Curvlet transform is a specifically defined mathematical transform, characterized by the parabolic scaling. Its generalization *width* is similar to the beam-aperture requirement for asymptotic beam solution: the beamwidth must be smaller than the scale of heterogeneity and much greater than the wavelength. Optimal beamwidth is reached by balancing the beam geometric spreading and the beam-front distortion. Using optimal beamwidth, beamlet or curvlet propagator will be sparse in smooth media for short-range propagation. For strong and rough heterogeneities, beamlet or curvlet scattering will occur and asymptotic propagator may not work well. In this case, the local perturbation method can be applied, in which the propagator is decomposed into a background propagator and a perturbation operator for each forward marching step. Numerical examples demonstrate the validity of the approach in this chapter.

Chapter 3: “Two-way Coupling of Solid-fluid with Discrete Element Model and Lattice Boltzmann Model” by Yucang Wang, Sheng Xue and Jun Xie.

This chapter presents a fully coupled solid-fluid code using Discrete Element Method (DEM) and Lattice Boltzmann Method (LBM). The new and distinctive features of this coupled approach compared with the existing coupled DEM-LBM models include the permission of bonded DEM particles, the capability to simulate explicitly fracturing events by the breakage of bonds, simulation of Darcy flow, free flow, and turbulent flow with the same integrated code, adoption of a more stable and efficient moving boundary condition, and a unified parallel algorithm for both codes based on MPI libraries, which allows larger scale parallel computing using super computers in the future. Two widely used open source codes, the Esys-Particle and OpenLB, are integrated as both of the codes are written using C++ and paralleled with MPI library. Recently, LBM has made a significant progress as a new method into numerical modeling of fluid dynamics. In contrast to the conventional computational fluid dynamics (CFD) techniques that solve macroscopic Navier-Stokes equations, LBM is built on a mesoscopic scale in which fluid is described by a group of discrete particles that propagate along a regular lattice and collide with each other. The use of LBM instead of CFD also eliminates severe mesh distortion due to frequent mesh geometry adaptation required in CFD. Because of its Eulerian grids, LBM is particularly suitable for modeling fluid-solid interaction problems, and a large number of solid particles can easily be accommodated.

Authors present three simple preliminary numerical results to assess the performance of the coupled DEM-LBM approach. The small scaled models are used as a qualitative display to demonstrate the capability and potential of the coupled approach. Some preliminary 2-D simulations, such as particles moving in the fluid, fluid flow in a narrow tunnel or crack and hydraulic fracture induced by the injection of fluid into a borehole, are carried out to validate the integrated code. These results show that the new method is capable of simulating solid particle flow in fluid, fluid flow inside narrow fracture, and hydraulic fracture by injection of fluid. The validation of large-scale simulations in 3-D and detailed comparisons with physical experiments are under development.

Chapter 4: “Co-seismic Damage and Post-Mainshock Healing of Fault Rocks at Landers, Hector Mine and Parkfield, California Viewed by Fault-Zone Trapped Waves” by Yong-Gang Li.

This chapter reviews fault rock co-seismic damage and post-mainshock healing progressions associated with the 1992 $M7.4$ Landers, the 1999 $M7.1$ Hector Mine, and the 2004 $M6.0$ Parkfield earthquakes in California through observations and 3-D finite-difference modeling of fault-zone trapped waves (FZTWs) generated by explosions and aftershocks, and recorded at linear seismic arrays deployed across and along the rupture zones (Li *et al.*, 1990, and further references). Because FZTWs arise from coherent multiple reflections at the boundaries between the low-velocity fault zone and the high-velocity surrounding rock, their amplitudes, frequencies and dispersive waveforms strongly depend on the fault geometry and physical properties, these waves enable to insight the internal structure and physical properties of fault zones at seismogenic depths with a higher resolution than ever before. The author with his colleagues from multiple institutions (see acknowledgement and references of Chapter 4) have used FZTWs to delineate the studied rupture zones being a low velocity waveguide about 100 to 250 m wide, in which S velocities are reduced by 40%–50% from wall-rock velocities and Q values are 10–50, which is interpreted as a remnant of process zone where inelastic deformation occurs around the propagating crack tip during dynamic rupture in the mainshocks. The width of the fault zone waveguide scales to the rupture length as predicted in published dynamic rupture models (e.g., Scholz, 1990). FZTWs also show the rupture segmentation and bifurcation associated with these earthquakes.

The strength of the low-velocity anomalies along the fault might vary over the earthquake cycle (e.g., Vidale *et al.*, 1994; Marone, 1998). Repeated seismic experiments conducted at the Landers rupture zone showed fault healing with recovery of seismic velocity by approximate 2% between 1994 and 1998. The survey in 1998 showed a reduction of the healing rate by a factor of two between 1994–1996 and 1996–1998. The ratio of the rates of P-wave and S-wave speed recovery is consistent with healing caused by closure of cracks that are partially fluid-filled. A similar experiment at Hector Mine has confirmed that healing is

not unique to Landers and shows that there is variability in healing rates among the fault segments that we have measured. However, the healing at the Landers rupture was interrupted in 1999 by the $M7.1$ Hector Mine earthquake rupture, which occurred 20–30 km away. The Hector Mine earthquake both strongly shook and permanently strained the Landers fault, adding damage discernible as a temporary reversal of the healing process. The fault has since resumed the trend of strength recovery that it showed after the Landers earthquake. These observations suggest that fault damage caused by strong seismic waves may help to explain earthquake clustering and seismicity triggering by shaking, and may be involved in friction reduction during faulting. At Parkfield, repeated surveys reveal an approximately 2.5% co-seismic decrease in seismic velocity within the San Andreas fault (SAF), due to the co-seismic damage of fault-zone rocks at seismogenic depths during dynamic rupture in the 2004 $M6$ Parkfield earthquake. Seismic velocities then increased by an approximate 1.2% in the following ~ 4 months, indicating that the rock damaged in the $M6$ mainshock recovers rigidity through time. These observations lead us to speculate that fault damage caused by strong seismic waves may help to explain earthquake clustering and seismicity triggering by shaking, and may be involved in friction reduction during faulting.

Chapter 5: “Subsurface Rupture Structure of the $M7.1$ Darfield and $M6.3$ Christchurch Earthquake Sequence Viewed with Fault-Zone Trapped Waves” by Yong-Gang Li, Gregory De Pascale, Mark Quigley and Darren Gravely.

In this chapter, Li *et al.* present the subsurface fault rock damage structure along the Greendale fault (GF) and Port Hills fault (PHF) that ruptured in the 2010 $M7.1$ Darfield and 2011 $M6.3$ Christchurch earthquake sequence using fault-zone trapped waves (FZTWs) generated by aftershocks recorded at a linear seismic array installed across the surface rupture along the GF. FZTWs were identified for aftershocks occurring on both the GF and the PHF. The post-S duration of these FZTWs increases as focal depths and epicentral distances from the array increase, showing an effective low-velocity waveguide formed by severely damaged rocks existing along the GF and PHF at seismogenic depths. Locations of aftershocks generating prominent FZTWs delineate the subsurface GF rupture extending eastward as bifurcating blind fault segments an additional ~ 5 –8 km beyond the mapped ~ 30 km surface rupture into a zone with comparably low seismic moment release west of the PHF rupture. The propagation of FZTW through the intervening ‘gap’ indicates moderate GF-PHF structural connectivity. This zone is interpreted as a fracture mesh reflecting the interplay between basement faults and stress-aligned microcracks that enable the propagation of PHF-sourced FZTWs into the GF damage zone.

Combined with previous rupture models for slip distributions in the Canterbury earthquake sequence (Quigley *et al.*, 2012; Barnhart *et al.*, 2011; Beavan *et al.*, 2012; Elliott *et al.*, 2012), authors construct a plausible model of subsurface

rupture zones associated with the Darfield-Christchurch earthquakes. Velocities of basement rocks in this model are constrained by the existing regional velocity models in Canterbury Plains (e.g., Smith *et al.*, 1995; Eberhart-Phillips and Bannister, 2002; Kaiser *et al.*, 2012). The 3-D finite-difference simulations of observed FZTWs suggest that the GF rupture zone is ~ 200 – 250 -m wide, consistent with the surface deformation widths, in which velocities are reduced by 35%–55% with the maximum reduction in the ~ 100 -m wide damage core zone corresponding to surface and shallow subsurface evidence for discrete fracturing. The damage zone delineated by FZTWs indicates an effective low-velocity waveguide extending ~ 65 km along the GF and PHF under the Canterbury Plains while the waveguide varies in its velocity and geometry along multiple rupture segments viewed by FZTWs, and penetrates down to the depth of ~ 8 km or deeper, consistent with hypocentral locations and geodetically-derived fault models. Their experiment also illuminates a potential approach to image the buried part of a rupture zone using FZTWs recorded at seismic array deployed at the surface-exposed part of the rupture zone.

Authors have examined the possible temporal change in wave velocity for repeated aftershock occurring just before and after the large aftershocks to find the additional co-seismic damage in rocks associated with these large aftershocks. We measured $\sim 2\%$ decrease of seismic velocity with fault rocks due to co-seismic damage by an $M5.3$ aftershock. This value is in general consistent with observations of fault rock damage and healing at the San Andreas fault associated with the 2004 $M6$ Parkfield earthquake (Li *et al.*, 2007, 2006).

Chapter 6: “Characterizing Pre-shock (Accelerating) Moment Release: A Few Notes on the Analysis of Seismicity” by Changsheng Jiang and Zhongliang Wu.

Understanding of seismicity is one of the frontiers in the modern seismology. Careful considerations in processing and analysis of seismicity using earthquake catalogues are necessary. In this chapter, Jiang and Wu demonstrate some useful tactics in analysis of earthquake catalog data and make notes on the existing methods used for careful analysis of seismicity in terms of (1) interfering events and the eclipse method, (2) the Bayesian information criterion, (3) the spatio-temporal scales for the sampling of seismic events, and (4) removal of aftershocks and the de-clustered Benioff strain method.

Authors use the pre-shock accelerating moment release (AMR) model (Bufe *et al.*, 1994; Brehm and Braile, 1998; Bowman and King, 2001) related to the critical-point-like behavior of earthquake preparation (Sornette and Sammis, 1995; Bowman *et al.*, 1998; Jaumé and Sykes, 1999; Rundle *et al.*, 2000). They explore whether the claimed and controversial pre-shock acceleration have a firm statistical (and seismological) basis by retrospective investigation in which they focus on the scaling exponent with the failure time fixed to the origin time of the ‘target’ earthquake so that the fitting can be stabilized by reducing one free

parameter (origin time). Borrowing from the concept of modern astronomy for analyzing remote planets, they use an ‘eclipse method’ for screening out the seismicity in the neighboring active fault zones as shown in analysis of seismicity for the 2008 *M*8 Wenchuan earthquake catalog data. The Bayesian Information Criterion (BIC) consideration provides a useful aid to judge whether the apparent ‘accelerating’ trend is statistically significant. The BIC criterion may be able to reveal more clues regarding the accelerating/quiescence behavior in the seismic moment release. To de-cluster an earthquake catalogue, previous works on AMR tended to use simple schemes (e.g., Robinson, 2005; Jiang and Wu, 2010), an alternative approach is to use the ‘Epidemic-Type Aftershock Sequences’ (ETAS) model (Ogata, 1988; Zhuang *et al.*, 2002; Zhuang and Ogata, 2006), in which a stochastic de-clustering scheme is proposed no longer determine whether an earthquake is a ‘background event’ or if it is triggered by another. To check the accelerating behavior objectively, authors also try to map the scaling coefficient calculated for different spatio-temporal windows, with different cutoff magnitude of the catalog (Jiang and Wu, 2005, 2010). The method extends a manifestation of the Gutenberg-Richter’s law. Deviation from the G-R power-law relation can be used for judging the completeness of an earthquake catalogue. Quantitatively, the goodness of fit between a power law fit to the data and the observed frequency-magnitude distribution as a function of a lower cutoff of the magnitude can be used (Wiemer and Wyss, 2000). Finally, they provide the case study in seismicity analysis using real catalog data: (1) ‘crack-like’ spatial window for the 2008 *M*8.0 Wenchuan earthquake, (2) a finite earthquake rupture of the 2004 *M*9.1 Sumatra-Andaman earthquake, and (3) seismic moment tensors to investigate the moment release before the 2011 *M*9.0 Tohoku earthquake.

Chapter 7: “Statistical Modeling of Earthquake Occurrences Based on External Geophysical Observations: With an Illustrative Application to the Ultra-low Frequency Ground Electric Signals Observed in the Beijing Region” by Jiancang Zhuang, Yoshihiko Ogata, David Vere-Jones, Li Ma and Huaping Guan.

In this chapter, authors present the idea on developing models for earthquake probability forecasts based on the precursor data from observations of the ultra-low frequency components of the underground electric signals used as an example to illustrate the modeling strategies. In the study case, signals from 4 stations in the vicinity of Beijing are used to monitor the variations in ultra-low frequency components electric field for forecasting the occurrence of $M \geq 4$ earthquakes within a 300-km circle centered in Beijing. The model used is a version of Ogata’s Lin-Lin algorithm for examining the influence of an explanatory signal on the occurrence of events in a stochastic point process, which is highly significant, and greatly superior to the explanatory effect of the same signals applied to a randomized version of the earthquake data. The results from all four stations show significant explanatory power although in combination the two most effective tend to dominate the forecasts. The predictions appear to

be most effective for events with $M \geq 5$, for which probability gains are up to 3–4 over the simple Poisson process, and for the events closer to the observing stations. Some smaller events appear to produce detectable signals at distances of over 100 km from the source.

The probability modeling framework adapted in this chapter is extended to the development of probability forecasts, which can be assessed directly, and in their turn can form the basis for a variety of decision procedures (e.g., Vere-Jones, 1995, and further references). Authors present a brief discussion of the performance of probability forecasts based on the best Lin-Lin model, which provides a strong confirmation of the reality of the explanatory power of the electric signals. They also carefully examine the effect of changes in background seismicity. Results show that the Lin-Lin model based on the electrical signals still out-performs the two-stage Poisson model.

The purpose of this book is to introduce the new approaches in solid-earth geophysics research with case studies. The following new methods and results presented in this book will be of particular interest to the readers:

- The full-3D waveform tomography method, and beamlets and curvelets methods for imaging complex subsurface structure.
- Observations and 3-D finite-difference simulations of fault-zone trapped wave for high-resolution delineation of fault internal structure and physical properties.
- Co-seismic rock damage and post-mainshock heal in major earthquakes.
- Discrete element method for solid-fluid coupling mechanics in earthquake fracture modeling.
- Pre-shock accelerating moment release with analysis of seismicity for earthquake risk assessment.
- Ultra-low frequency ground electric signals for statistical modeling of earthquake occurrences.

This book is a self-contained volume starting with an overview of the subject then explores each topic with in depth detail. Extensive reference lists and cross references with other volumes to facilitate further research. Full-color figures and tables support the text and aid the readers in understanding. Content is suited for both the senior researchers and graduate students in geosciences who will broaden their horizons about observational, computational and applied seismology and earthquake sciences. This book covers multi-disciplinary topics to allow readers to grasp the new methods and techniques used in data analysis and numerical modeling for structural, physical and mechanical interpretation of earthquake phenomena, to aid the understanding of earthquake processes and hazards, and thus helps readers to evaluate potential earthquake risk in seismogenic regions globally.